Materials Research. 2010; 13(4): 485-495

ZrO_2 Nanoparticles' Effects on Split Tensile Strength of Self Compacting Concrete

Ali Nazari*, Shadi Riahi

Department of Technical and Engineering Sciences,
Islamic Azad University (Saveh Branch), Saveh, Iran

Received: July 18, 2010; Revised: September 9, 2010

In the present study, split tensile strength of self compacting concrete with different amount of ZrO_2 nanoparticles has been investigated. ZrO_2 nanoparticles with the average particle size of 15 nm were added partially to cement paste (Portland cement together with polycarboxylate superplasticizer) and split tensile strength of the specimens has been measured. The results indicate that ZrO_2 nanoparticles are able to improve split tensile strength of concrete and recover the negative effects of polycarboxylate superplasticizer. ZrO_2 nanoparticle as a partial replacement of cement up to 4 wt. (%) could accelerate C-S-H gel formation as a result of increased crystalline $Ca(OH)_2$ amount at the early age of hydration. The increased the ZrO_2 nanoparticles' content more than 4 wt. (%), causes the reduced the split tensile strength because of unsuitable dispersion of nanoparticles in the concrete matrix.

Keywords: *A. Ceramic-matrix composites (CMCs), A. Nano particles, D. Scanning electron microscopy (SEM), D. Thermogravimetric analysis (TGA), D. X-ray diffraction (XRD)*

1. Introduction

Self-compacting concrete (SCC) is one of the most significant advances in concrete technology in recent years. SCC may be defined as a concrete with the capacity to flow inside the formwork, to pass around the reinforcements and through the narrow sections, consolidating simply under its own weight without needing additional vibration and without showing segregation or bleeding. This behavior is achieved in normally vibrated concretes (NVC) in which the same components are used with a higher content of fines and using very powerful superplasticizers. In addition, to increase the viscosity of the paste, viscosity-modifying admixtures can also be used. These are usually comprised of polymers made up of long-chain molecules which are capable to absorb and fix the free water content. This modification in the mix design may have an influence on the mechanical properties of materials; therefore it is important to ensure that all of the basic assumptions and test results for design models of NVC construction are also valid for SCC construction.

Most articles which are published until now show that for a certain compressive strength, SCC tends to reach strength slightly higher than type of NVC[1-3]. Nearly, all research has used SCC, which includes active additions to satisfy the great demand for fines are needed for this type of concrete, thereby, improving their mechanical properties in comparison with NVC. For instance, Köning et al.[1] and Hauke[2] registered strength increase in SCCs made with different amount of fly ash. According to Fava et al.[3], in SCCs with granulated blast furnace slag, this increasing is also evident. On the other hand, when limestone filler is used, Fava et al.[3] and Daoud et al.[4] achieved a tensile strength in SCC lower than that type of NVC. Bolsjkov[5] has illustrated the behavior of both types of concrete are similar. As for the modulus of elasticity, it is generally seen that this rises with age at a similar rate to that of NVCs[1], though it seems that SCCs are a little more deformable[6-9]. These small differences in stiffness between the two types of concrete can be attributed to the SCCs' high paste content; although according to Su et al.[10] increasing the fine aggregate/total aggregate ratio does not have a significant effect on the SCCs' modulus of elasticity. In any case, it should be pointed out that most of the results are available in the bibliography usually refer to highly strength SCCs, where high cement contents (higher than 400 $kg.m^{-3}$) are used to be usually accompanied by active additions, such as fly ash or blast furnace slag. However, there are few studies that give results of low to medium compressive strength with SCCs.

As authors knowledge, there are few works on incorporating nanoparticles into SCCs to achieve improved physical and mechanical properties. Only, there are several reports on incorporation of nanoparticles in NVCs which most of them have focused on using SiO_2 nanoparticles[11-20]. In addition, some of the works have conducted on utilizing nano-Al_2O_3[21,22], nano-Fe_2O_3[23] and zinc-iron oxide nanoparticles[24]. Previously, a series of works[25-32] has been conducted on cementitious composites by adding different nanoparticles evaluating the mechanical properties of the composites.

Incorporating of other nanoparticles is rarely reported. Therefore, introducing some other nanoparticles which probably could improve the mechanical and physical properties of cementitious composites is inherent. The aim of this study is incorporating ZrO_2 nanoparticles into SCCs to study tensile strength and pore structure of the concrete. Several specimens with different amount of polycarboxylate superplasticizer (PC) have been prepared and their physical and mechanical properties have been considered when, instead of cement, ZrO_2 nanoparticles were partially added to the cement paste.

2. Materials and Methods

Ordinary Portland Cement (OPC) conforming to ASTM C150[33] standard was used as received. The chemical and physical properties of the cement are shown in Table 1. The particle size distribution pattern of the used OPC has been illustrated in Figure 1.

ZrO_2 nanoparticles with average particle size of 15 nm and 45 $m^2.g^{-1}$ Blaine fineness producing from Suzhou Fuer Import & Export Trade Co., Ltd was used as received. The properties of ZrO_2 nanoparticles are shown in Table 2. Scanning electron micrographs (SEM) and powder X-ray diffraction (XRD) diagrams of ZrO_2 nanoparticles are shown in Figures 2 and 3.

*e-mail: alinazari84@aut.ac.ir

Crushed limestone aggregates were used to produce self-compacting concretes, with gravel 4/12 and two types of sand: one coarse 0/4, for fine aggregates and the other fine 0/2, with a very high fines content (particle size < 0.063 mm) of 19.2%, the main function of which was to provide a greater volume of fine materials to improve the stability of the fresh concrete.

A polycarboxylate with a polyethylene condensate defoamed based admixture (Glenium C303 SCC) produced from Muhu (China) Construction Materials Co., Ltd was used. Table 3 shows some of the physical and chemical properties of polycarboxylate admixture used in this study.

Totally, two series of mixtures were prepared in the laboratory trials. C0-SCC series mixtures were prepared by cement, fine and ultra-fine crushed limestone aggregates with 19.2% by weight of ultra-fine ones and 0, 0.3, 0.5, 0.7 and 1.0% by weight of polycarboxylate admixture replaced by water. N-SCC series were prepared with different contents of ZrO_2 nanoparticles with average particle size of 15 nm. The mixtures were prepared with the cement replacement by ZrO_2 nanoparticles from 1 to 5 wt. (%) and 1 wt. (%) polycarboxylate admixture. The water to binder ratio for all mixtures was set at 0.40[34]. The binder content of all mixtures was 450 kg.m^{-3}. The proportions of the mixtures are presented in Table 4.

The mixing sequence for SCCs was consisted of homogenizing the sand and cementitious materials for one minute in the mixer and then approximately 75% of the mixing water was added. The coarse aggregate was introduced and then the superplasticizer was pre-dissolved in the remaining water and was added at the end of the mixing sequence. The total mixing time including homogenizing was 5 minutes.

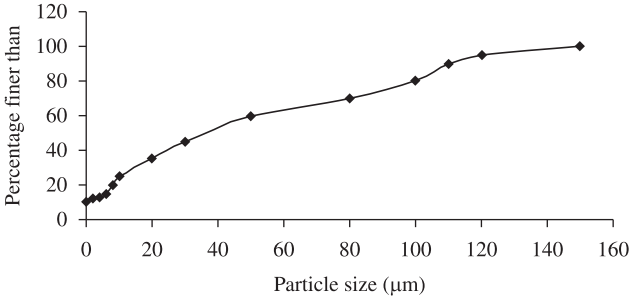

Figure 1. Particles distribution pattern of ordinary Portland cement.

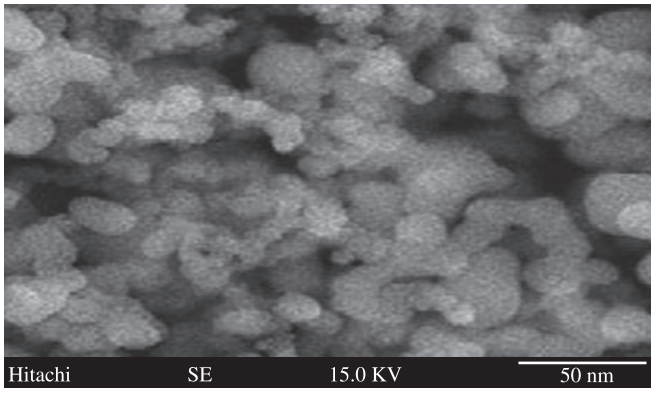

Figure 2. SEM micrograph of ZrO_2 nanoparticles.

Several types of tests were carried out on the prepared specimens:

- *Split tensile strength*: Cylindrical specimens with the diameter of 150 mm and height of 300 mm were made for split tensile tests. The moulds were covered with polyethylene sheets and moistened for 24 h. Then the specimens were demoulded and cured in water at a temperature of 20 °C in the room condition prior to test days. The split tensile strength tests of the samples were determined at 2, 7 and 28 days of curing. Split tensile tests were carried out according to the ASTM C 496[35] standard. The tests were carried out triplicately and average split tensile strength values were obtained;
- *Mercury intrusion porosimetry:* There are several methods generally used to measure the pore structure, such as optics method, mercury intrusion porosimetry (MIP), helium flow and gas adsorption[36]. MIP technique is extensively used to characterize the pore structure in porous material as a result of its simplicity, quickness and wide measuring range of pore diameter[36,37]. MIP provides information about the connectivity of pores[36]; and
- In this study, the pore structure of concrete is evaluated by using MIP. To prepare the samples for MIP measurement, the concrete specimens after 28 days of curing were first broken into smaller pieces, and then the cement paste fragments selected from the center of prisms were used to measure pore structure. The samples were immersed in acetone to stop hydration as fast as possible. Before mercury intrusion test, the samples were dried in an oven at about 110 °C until constant weight to remove moisture in the pores. MIP is based on the assumption that the non-wetting liquid mercury (the contact angle between mercury and solid is greater than 90°) will only intrude in the pores of porous material under pressure[36,37]. Each pore size is quantitatively determined from the relationship between the volume of intruded mercury and the applied pressure[37]. The relationship between the pore diameter and applied pressure is generally described by Washburn equation as follows[36,37]:

$$D = -4\gamma\cos\theta / P \quad (1)$$

where:

D is the pore diameter (nm);
γ is the surface tension of mercury (dyne.cm^{-1});
θ is the contact angle between mercury and solid (°); and
P is the applied pressure (MPa).

The test apparatus used for pore structure measurement is Auto Pore III mercury porosimeter. Mercury density is 13.5335 g.mL^{-1}. The surface tension of mercury is taken as 485 dynes.cm^{-1}, and the contact angle selected is 130°. The maximum measuring pressure applied is 200 MPa (30000 psi), which means that the smallest pore diameter that can be measured reaches about 6 nm (on the assumption that all pores have cylindrical shape).

Table 1. Chemical and physical properties of Portland cement wt. (%).

Material	SiO_2	Al_2O_3	Fe_2O_3	CaO	MgO	SO_3	Na_2O	K_2O	Loss on ignition
Cement	21.89	5.3	3.34	53.27	6.45	3.67	0.18	0.98	3.21

Specific gravity: 1.7 g.cm^{-3}.

- *Conduction calorimetry:* The test was run out on a Wexham Developments JAF model isothermal calorimeter, using IBM program AWCAL-4, at 22 °C for a maximum of 70 hours. Fifteen grams of cement was mixed with water and saturated limewater and admixture before introducing it into the calorimeter cell.
- *Thermogravimetric analysis (TGA):* A Netzsch model STA 409 simultaneous thermal analyzer equipped with a Data Acquisition System 414/1 programmer was used for the tests. Specimens which were cured for 28 days were heated from 110 to 650 °C, at a heating rate of 4 °C/min and in an inert N_2 atmosphere.
- *Scanning electron microscopy (SEM)*: SEM investigations were conducted on a Hitachi apparatus. Backscattered electron (BSE) and secondary electron (SE) imaging was used to study the samples, which were prepared under conditions that ensured their subsequent viability for analytical purposes.
- *X-ray diffraction (XRD):* A Philips PW-1730 unit was used for XRD analysis which was taken from 4 to 70°.

3. Results and Discussion

3.1. Strength analysis of C0-SCC specimens

Figure 4 shows the split tensile strength of C0-SCC specimens after 2, 7 and 28 days of curing which are all reduced by increasing PC amount especially at early age of curing. This fact may be due to various factors, such as using different superplasticizers or greater fines content in the SCCs. Roncero and Gettu[38] have pointed out the formation of large CH crystals by using polycarboxylate superplasticizers. These large crystals weaken the aggregate-paste transition zone and hence decrease the tensile strength of concrete by decreasing the aggregate-paste bond. As for the influence of the fines content, the bigger this is the greater the shrinkage becomes[8,39-43], giving rise to the appearance of a greater number of micro-cracks in the aggregate paste interface which also reduce the tensile strength. Moreover, by increasing the volume of fines, the specific surface area of the aggregates increases, with the aggregate-paste transition zone is being precisely the weakest phase of the concrete.

During the early days of hydration, the strength is affected by two opposing effects: on one hand, the limestone fines raise the rate of hydration of some clinker compounds since the fines act as nucleation sites of the hydrates formed in the hydration reactions[5,44]. On the other hand, PC has a delaying effect on hydration of CH crystals and formation of C_3H[45,46].

At higher ages, 28 days, the two aforementioned effects disappear and it can clearly be seen that there is less effects on reducing the split tensile strength in SCCs by increasing PC. This is due to a longer development over time for the cement's hydration processes in the SCCs with higher content of PC as a result of the SCCs' greater capacity to retain water[47], which allows pozzolanic additions to continue reacting at higher ages with the lime resulting from the cement hydration. Furthermore, although PC retards the initial hydration reactions, according to Puertas et al.[47] these reactions are intensified in later stages as a result of particle dispersion.

The pore structure of concrete is the general embodiment of porosity, pore size distribution, pore scale and pore geometry. The test results of MIP in this study include the pore structure parameters such as total specific pore volume, most probable pore diameter, pore size distribution, porosity, average diameter, and median diameter (volume). In terms of the different effect of pore size on concrete performance, the pore in concrete is classified as harmless pore (< 20 nm), few-harm pore (20~50 nm), harmful pore (50~200 nm) and multi-harm pore (>200 nm)[48]. In order to analyze and compare conveniently, the pore structure of concrete is divided into four ranges according to this sort method in this work.

Table 5 shows that with increasing PC content, the total specific pore volumes of concretes are decreased, and the most probable pore diameters of concretes shift to smaller pores and fall in the range of

Table 2. The properties of ZrO_2 nanoparticles.

Diameter (nm)	Surface volume ratio ($m^2.g^{-1}$)	Density ($g.cm^{-3}$)	Purity (%)
15 ± 3	165 ± 12	< 0.15	>99.9

Table 3. Physical and chemical characteristics of the polycarboxylate admixture.

Appearance	Yellow-brown liquid
% solid residue	Approximately 36%
pH	5.2-5.3
Specific gravity ($kg.L^{-1}$)	Approximately 1.06
Rotational Viscosity (MPa)	79.30
% C	52.25
ppm Na^+	9150
ppm K^+	158

Table 4. Mixture proportion of nano- ZrO_2 particles blended concretes.

Sample designation	ZrO_2 nanoparticles (%)	PC content (%)	Quantities ($kg.m^{-3}$)	
			Cement	ZrO_2 nanoparticles
C0-SCC0	0	0	450	0
C0-SCC0.3	0	0.3	450	0
C0-SCC0.5	0	0.5	450	0
C0-SCC0.7	0	0.7	450	0
C0-SCC1	0	1.0	450	0
N1-SCC1	1	1.0	445.5	4.5
N2-SCC1	2	1.0	441.0	9.0
N3-SCC1	3	1.0	437.5	13.5
N4-SCC1	4	1.0	432.0	18.0
N5-SCC1	5	1.0	427.5	22.5

Water to binder [cement + nano- ZrO_2] ratio of 0.40.

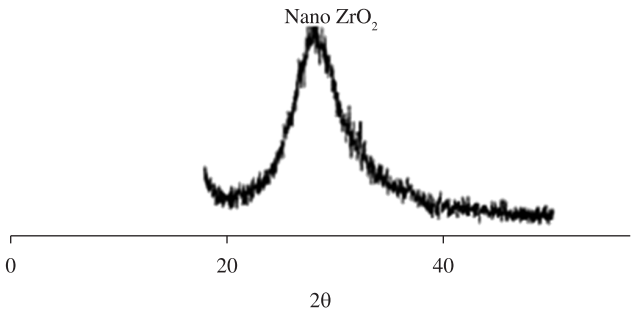

Figure 3. XRD analysis of ZrO_2 nanoparticles.

Table 5. Properties of the pores in C0-SCC and N-SCC specimens.

Sample designation	Total specific pore volume ($mL.g^{-1}$)	Most probable pore diameter (nm)	Porosity (%)	Average diameter (nm)	Median diameter (volume) (nm)	Pore size distribution ($mL.g^{-1}(\%)$)			
						Pore size distribution ($mL.g^{-1}(\%)$)	Few-harm pores (20~50 nm)	Harmful pores (50~200 nm)	Multi-harm pores (>200 nm)
C0-SCC0	0.0381	32	8.99	27.53	41.4	0.0045	0.0127	0.0149	0.0079
C0-SCC0.3	0.0346	24	8.11	20.9	30.3	0.0044	0.0116	0.0121	0.0064
C0-SCC0.5	0.0332	20	7.70	16.8	28.7	0.0043	0.0108	0.0114	0.0056
C0-SCC0.7	0.0320	18	7.46	12.1	25.4	0.0041	0.0101	0.0108	0.0045
C0-SCC1	0.0304	14	7.17	10.2	22.2	0.0039	0.0090	0.0100	0.0038
N1-SCC1	0.0272	11.4	6.60	9.5	20.23	0.0036	0.0084	0.0090	0.0272
N2-SCC1	0.0251	11.4	6.31	9.1	18.81	0.0034	0.0079	0.0084	0.0251
N3-SCC1	0.0233	10.4	6.11	8.5	15.68	0.0030	0.0071	0.0067	0.0233
N4-SCC1	0.0217	9.5	5.91	7.9	11.59	0.0027	0.0064	0.0048	0.0217
N5-SCC1	0.0227	10.4	5.99	8.2	13.87	0.0028	0.0067	0.0061	0.0227

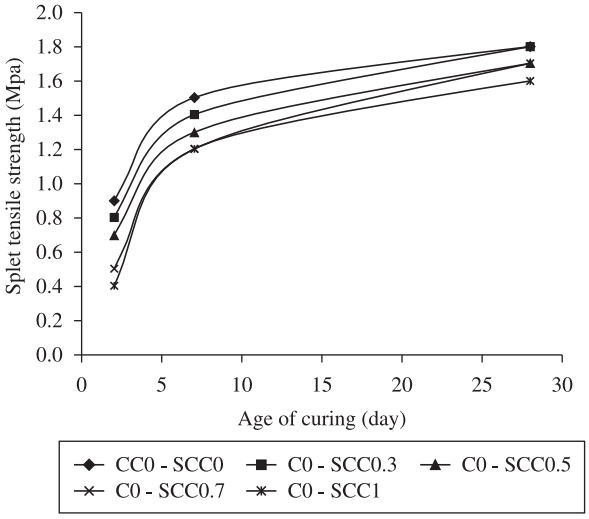

Figure 4. Split tensile strength of C0-SCC specimens.

few-harm pore, which indicates that the addition of PC refines the pore structure of concretes.

Table 5 gives the porosities, average diameters and median diameters (volume) of various concretes. The regularity of porosity is similar to that of total specific pore volume. The regularity of average diameter and median diameter (volume) is similar to that of most probable pore diameter.

The pore size distribution of concretes is shown in Table 5. It is seen that by increasing PC content, the amounts of pores decrease, which shows that the density of concretes is increased and the pore structure is improved.

Table 6 shows the conduction calorimetry of C0-SCC specimens. Two signals can be distinguished on all test results: a peak corresponding to the acceleration or post-induction period, associated with the precipitation of C–S–H gel and CH, and a shoulder related to a second, weaker signal with a later peak time, associated with the transformation from the ettringite (AFt) to the calcium monosulphoaluminate (AFm) phase via dissolution and reaction with $Al(OH)^{4-}$ [49]. The numerical values corresponding to these two signals (heat release rate, peak times) and the total released heat are shown in Table 6. The time period over the total heat was measured until the heat release rate was below 1% of the maximum of the second peak.

The heat release rate values in Table 6 show that increasing the percentage of PC in the pastes retards peak times and raises heat release rate values. This is indicative of a delay in initial cement hydration because of higher content of PC. The retardation is much less marked in the second peak. The total heat released under identical conditions (at times when the heat release rate is less than 1% of the maximum amount of heat released in the first peak) decreases with higher percentages of PC in the mix.

Table 7 shows the thermogravimetric analysis results of C0-SCC specimens measured in the 110-650 °C range in which dehydration of the hydrated products occurred. The results show that after 28 days of curing, the loss in weight of the specimens is increased by decreasing the PC content in concretes.

Figure 5 shows XRD analysis of C0-SCC specimens at different times after curing. As Figure 5 also shows, the peak related to formation of the hydrated products shifts to appear in later times indicating the negative impact of PC on formation of $Ca(OH)_2$ and C-S-H gel at early ages of cement hydration.

Finally, Figure 6 shows SEM micrographs of C0-SCC specimens without and with PC. The morphological analysis evinced no substantial differences in either the form or the texture of the different reaction products in pastes with and without admixtures. The micrographs corresponding to paste cured for 2 and 7 days show anhydrous cement that has not yet reacted, along with a relatively porous mass analogous to the reaction products. This region is more compact and less porous in the paste with admixture. After 28 days, the reaction is observed to progress, with a considerable decrease in the amount of anhydrous cement particles. The atomic ratios found in an analysis performed on the reaction products of all the pastes studied which are shown in Table 6.

The results obtained with respect to the effect of PC on cement hydration show that at early ages PC retards the initial cement hydration. This effect is more evident at higher doses of superplasticizer. This phenomenon is confirmed by the results obtained in conduction calorimetry, with a retardation of the peak time for the first peak in the heat release rate, associated with C_3H and CH formation. This lower initial formation of reaction products is further corroborated by the smaller weight loss detected in 2 days cured pastes with admixtures, when subjected to temperatures of

110-650 °C. Such weight loss is related to the partial and total dehydration of C_3H and CH.

The delay in hydration reactions is expressed as a very extensive lengthening of the initial and final setting times of the pastes that have high dosages of PC admixture. SNF and SMF superplasticizers also produce retardations in initial cement hydration reactions, a development that is closely associated to the adsorption of the compounds to the surface of cement particles or some of the hydration products[50]. PC admixtures likewise adsorb on the surface of cement particles, with a dispersive capability that is dependent upon the amount adsorbed. According to Yamada and Hanehara[51] such adsorption is affected by two important factors: the specific area of the solid phases and possible competition with other anionic species, such as sulphate ions, in the adsorption process[52].

In summary, in its interactions with the reactive species, the organic admixture affects hydrated phase diffusion, nucleation and growth and therefore the hydration process. Setting is related to the concentration of Ca^{2+} ions in the liquid phase: delayed setting is attributed to a decrease in the concentration of such Ca^{2+} ions. Using X-ray photoelectron spectroscopy or electron spectroscopy for chemical analysis (ESCA), Uchikawa et al.[53] showed that a chelate forms in pastes with PC admixtures as a result of the reaction between the Ca^{2+} ions and the admixture molecules. The formation of this chelate would inferior the Ca^{2+} concentration and thereby retards setting and hinders solid phase nucleation.

Differences of some significance were observed, however, in the porosity data: after 2 days of hydration, as the PC admixture content is increased, total porosity is declined and the pore structure became more refined, with a rise in the percentage of mesopores and a decline in the macropore contents. Roncero et al.[54] have reported similar results, observing a decrease in total porosity and in the distribution of pore size in cement pastes which contains different types of superplasticizer admixtures (a polycarboxylate admixture among them). Their results refer to pastes cured at 7 and 28 days.

This, in turn, would explain the lengthening of the induction period observed in the heat release rate when the content of the PC admixture is increased (Table 6). Jolicoeur and Simard[55] have found similar results with more conventional superplasticizers. This retardation of C_3H and CH nucleation and growth is the reason for the higher weight loss obtained with thermogravimetric analysis (Table 7) in 28-day pastes containing more PC admixture.

Table 6. Calorimetric results of C0-SCC and N-SCC specimens.

Sample designation	Total heat	First peak		Second peak	
	$kJ.kg^{-1}$	Time (hours)	Rate ($W.kg^{-1}$)	Time (hours)	Rate ($W.kg^{-1}$)
C0-SCC0	319.8	1.8	0.62	16.1	2.71
C0-SCC0.3	333.5	1.9	0.64	17.2	2.86
C0-SCC0.5	345.3	2.1	0.67	18.6	3.02
C0-SCC0.7	359.5	2.25	0.69	19.5	3.29
C0-SCC1	371.7	2.4	0.71	20.6	3.41
N1-SCC1	308.2	2.1	0.617	16.6	2.69
N2-SCC1	281.6	1.8	0.579	15.5	2.38
N3-SCC1	267.1	1.5	0.551	13.8	2.11
N4-SCC1	246.8	1.1	0.503	12.2	1.90
N5-SCC1	260.8	1.4	0.522	13.1	2.04

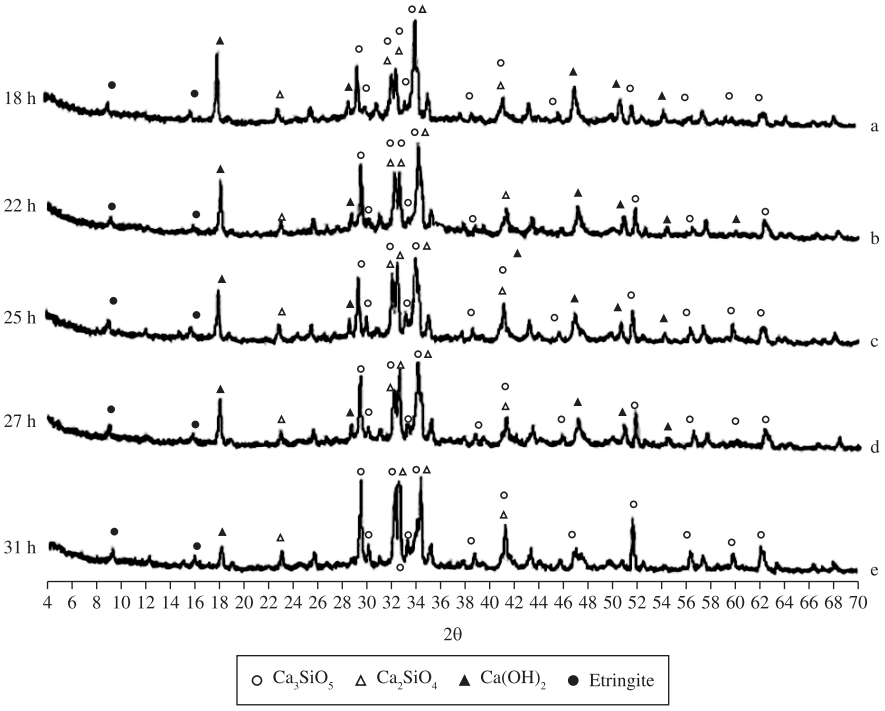

Figure 5. XRD results indicating the formation of hydrated products for different C0-SCC specimens: a) C0-SCC0; b) C0-SCC0.3; c) C0-SCC0.5; d) C0-SCC0.7; and e) C0-SCC1.

Table 7. Weight loss (%) of the pastes in the range of 110-650 °C at 28 days of curing of C0-SCC and N-SCC specimens.

Sample designation	Total heat
	$kJ.kg^{-1}$
C0-SCC0	10.4
C0-SCC0.3	10.7
C0-SCC0.5	11.0
C0-SCC0.7	11.2
C0-SCC1	11.4
N1-SCC1	10.6
N2-SCC1	10.5
N3-SCC1	10.2
N4-SCC1	10.1
N5-SCC1	9.9

The presence of admixtures does not seem to affect the mechanical strength of the paste at either 2 or 28 days of hydration (Figure 4). After 2 days, the pastes with superplasticizer have smaller amounts of reaction products (C–S–H gel and Ch crystals), their mechanical behavior appears to be more tightly is related to the pore structure (decrease in the size of the pores) and, very likely, to a better distribution of the different components. Legrand and Warquin[56] have found that in the presence of superplasticizers, despite a decrease in hydrate formation, strengths were comparable, and explained this development by the better dispersion of cement particles. Therefore, only cement paste with 1 wt. (%) PC admixture was selected because of its high workability and cement was partially replaced by different amount of ZrO_2 nanoparticles. The results are discussed in the following section.

3.2. Strength analysis of N-SCC specimens

Figure 7 shows the split tensile strength of N-SCC specimens after 2, 7 and 28 days of curing. The results show that the split tensile strength increases by adding ZrO_2 nanoparticles up to 4 wt. (%) replacement (N4-SCC series) and then it decreases, although adding 5% ZrO_2 nanoparticles produces specimens with much higher split tensile strength with respect to the all other C0-SCC concretes. The reduced split tensile strength by adding more than 4 wt. (%) ZrO_2 nanoparticles may be due to this fact that the quantity of ZrO_2 nanoparticles present in the mix is higher than the amount required to combine with the liberated lime during the process of hydration thus leading to excess silica leaching out and causing a deficiency in strength as it replaces part of the cementitious material but does not contribute to strength. Also, it may be due to the defects generated in dispersion of nanoparticles that causes weak zones.

The higher split tensile strength in the N-SCC series mixtures with respect to C0-SCC series is due to the rapid consumption of crystalline $Ca(OH)_2$ which quickly are formed during hydration of Portland cement specially at early ages as a result of high reactivity of ZrO_2 nanoparticles. As a consequence, the hydration of cement is accelerated and larger volumes of reaction products are formed. Also ZrO_2 nanoparticles recover the particle packing density of the blended cement, directing to a reduced volume of larger pores in the cement paste.

Table 5 shows that with increasing ZrO_2 nanoparticles up to 4 wt. (%), the total specific pore volumes of concretes are decreased, and the most probable pore diameters of concretes shift to smaller pores and fall in the range of few-harm pore, which indicates that the addition of PC refines the pore structure of concretes.

Table 5 gives the porosities, average diameters and median diameters (volume) of various concretes. The regularity of porosity is similar to that of total specific pore volume. The regularity of average diameter and median diameter (volume) is similar to that of most probable pore diameter.

The pore size distribution of concretes is shown in Table 5. It is observed that by adding nanoparticles, the amounts of pores decreased, which shows that the density of concretes is increased and the pore structure is improved.

The effectiveness of nano-ZrO_2 in improving the pore structure of concretes increases in the order: N1-SCC <N2-SCC <N3-SCC <N5-SCC <N4-SCC. With increasing the nanoparticles' content, the reduced extent of pores in concretes is all decreased, and the improvement on the pore structure of concretes is weakening.

The mechanism that the nanoparticles improve the pore structure of concrete can be interpreted as follows[57]: Suppose that nanoparticles are uniformly dispersed in concrete and each particle is contained in a cube pattern, therefore the distance between nanoparticles can be determined. After the hydration begins, hydrate products diffuse and envelop nanoparticles as kernel[57]. If the content of nanoparticles and the distance between them are appropriate, the crystallization will be controlled to be a suitable state through restricting the growth of $Ca(OH)_2$ crystal by nanoparticles. Moreover, the nanoparticles located in cement paste as kernel can further promote cement hydration due to their high activity. This makes the cement matrix more homogeneous and compact. Consequently, the pore structure of concrete is improved evidently such as the concrete containing nano-ZrO_2 in the amount of 1% by weight of binder[57].

With increasing the content of ZrO_2 nanoparticles more than 4 wt. (%), the improvement on the pore structure of concrete is weakened. This can be attributed to that the distance between nanoparticles decreases with increasing content of nanoparticles, and $Ca(OH)_2$ crystal cannot grow up enough due to limited space and the crystal quantity is decreased, which leads to the ratio of crystal to strengthening gel small and the shrinkage and creep of cement matrix increased[58], thus the pore structure of cement matrix is looser relatively.

On the whole, the addition of nanoparticles improves the pore structure of concrete. On the one hand, nanoparticles can act as a filler to enhance the density of concrete, which leads to the porosity of concrete reduced significantly. On the other hand, nanoparticles can not only act as an activator to accelerate cement hydration due to their high activity, but also act as a kernel in cement paste which makes the size of $Ca(OH)_2$ crystal smaller and the tropism more stochastic.

The heat release rate values in Table 6 show that increasing the percentage of ZrO_2 nanoparticles up to 4 wt. (%) in the pastes accelerates peak times and drops heat release rate values. This is indicative of acceleration in initial cement hydration due to higher content of ZrO_2 nanoparticles. ZrO_2 nanoparticles as a foreign nucleation site can accelerate the cement hydration and hence increase the heat release rate. As it is stated above, the appearance of the peaks in conduction calorimetry tests are due to CH and C_3H compounds formation in the cement paste. When ZrO_2 nanoparticles partially added to cement paste, the acceleration in formation of CH and C_3H would result in more rapid appearance of the related peaks.

Table 7 shows the thermogravimetric analysis results of N-SCC specimens measured in the 110-650 °C range in which dehydration of the hydrated products occurred. The results show that after 28 days of curing, the loss in weight of the specimens is increased by increasing ZrO_2 nanoparticles in concretes up to 4 wt. (%). Again,

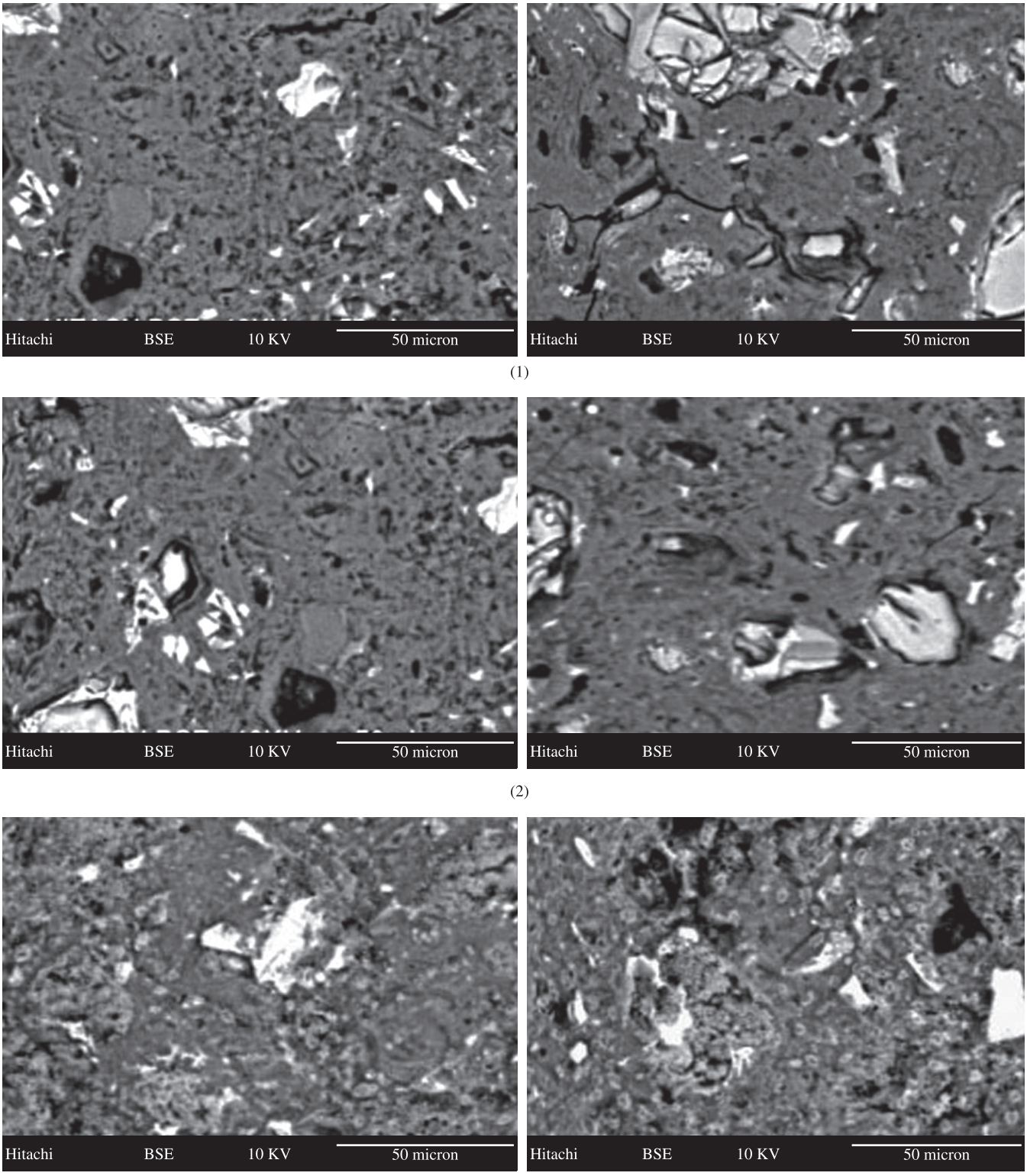

Figure 6. SEM micrographs of a) C0-SCC0 specimen and b) C0-SCC1 specimen at 2 days (series 1), 7 days (series 2) and 28 days (series 3) of curing.

such as the results obtained for conduction calorimetry, the increase in loss weight is due to more formation of CH and C_3H compounds in the cement paste.

Figure 8 shows XRD analysis of N-SCC specimens at different times after curing. As Figure 8 also shows, the peak related to formation of the hydrated products shifts to appear in earlier times indicating the positive impact of PC on formation of $Ca(OH)_2$ and C-S-H gel at early age of cement hydration.

Finally, Figure 9 shows SEM micrographs of N-SCC specimens containing 4 wt. (%) of ZrO_2 nanoparticles. Figure 9 shows a more

compact mixture after all days of curing which indicate rapid formation of C-S-H gel in presence of ZrO_2 nanoparticles.

In this paper, the strength enhancement under compression force has been investigated energetically:

Both nanoparticles and aggregates are exterior components but, why the nanoparticles are able to make a stronger composite is as a result of the free energy of nucleation sites. The driving force for the nucleation is the reduction of interfacial free energy between the nucleus (C-S-H gel) and nucleation site (nanoparticle or aggregates).

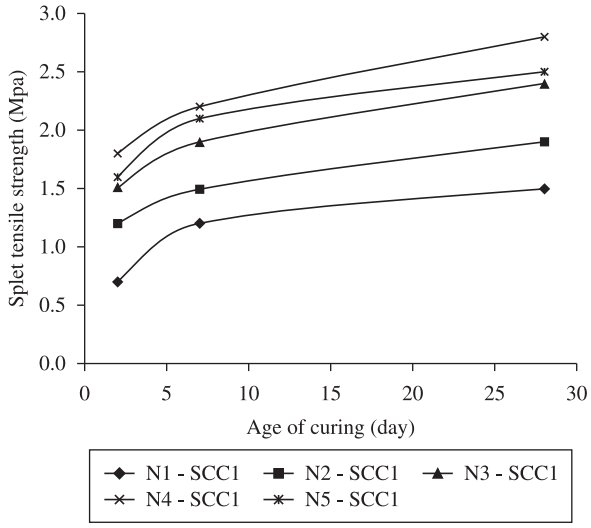

Figure 7. Split tensile strength of N-SCC specimens.

In comparison between these two approximately spherical particles (nanoparticle and aggregates), the ratio between surface area to volume of nanoparticle is much larger than that of aggregates. Therefore, the abiltity of the nanoparticle to formation of C-S-H gel is more than this for aggregates.

In addition, the C-S-H gel-nanoparticle interface is probably coherent or semi-coherent. This is due to this fact that C-S-H gel formed around the nanoparticle could maintain its coherency with nanoparticle because both C-S-H gel and nanoparticle have nano-scale dimensions. But the C-S-H gel formed around the aggregate has a completely incoherent interface with aggregate. In the other words, the sand particle is large enough which could not maintain its coherency with nanoscale C-S-H gel. Furthermore, in the vicinity of the aggregates, the probability of void formation and presence of un-reacted cement, other aggregates and even nanoparticles is much more with respect to the nanoparticle causes more weak zones in the vicinity of sand. Although sands act as reinforcement in cementitious matrix but as a result of incoherency under split tensile loading, fracture occurrence and crack propagation from the C-S-H gel formed at the surface of the sand is more probable with respect to the nanoparticle. This phenomenon is tightly like to the inclusions and precipitations in metallic alloys where inclusions with incoherent interface (like aggregate in concrete) could not improve the mechanical properties of the alloy while precipitations with coherent or semi-coherent interface (like nanoparticle in concrete) could improve mechanical properties of the alloy mainly. Therefore, the smaller the nanoparticle size, the more the heterogeneous nucleation sites results in shorter early age according to Equation 1[59,60]:

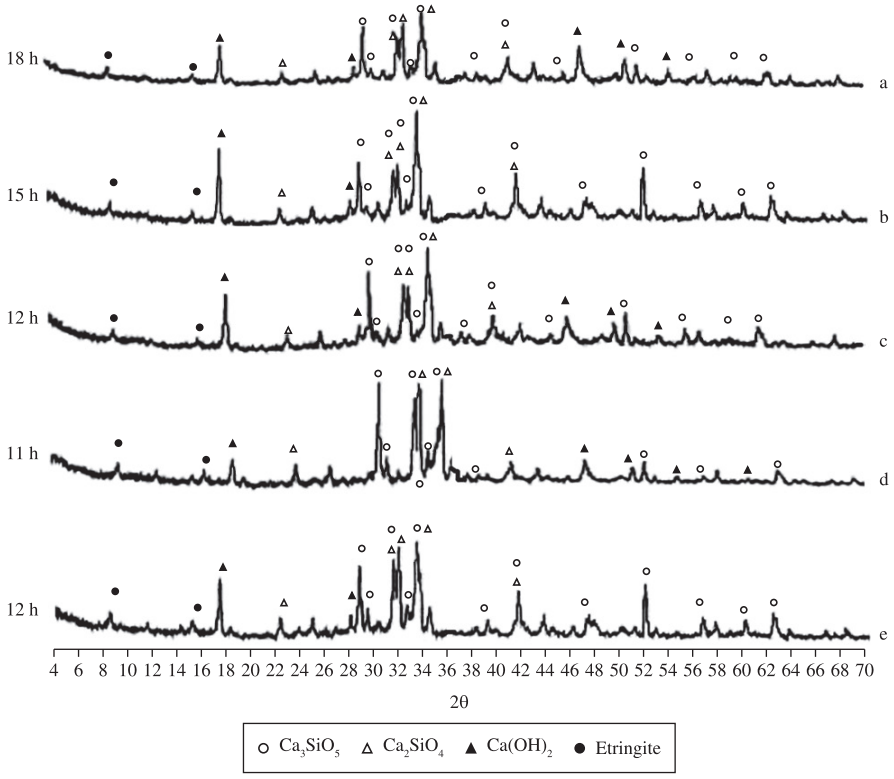

Figure 8. XRD results indicating the formation of hydrated products for different N-SCC specimens: a) N1-SCC1; b) N2-SCC1; c) N3-SCC1; d) N4-SCC1; and e) N5-SCC1.

$$I = A.N_T.\exp\left(\frac{-\Delta G^*}{KT}\right) \quad (1)$$

where:

I [nucleus/s] is the nucleation rate;

ΔG* [J] is the critical free energy for nucleation;

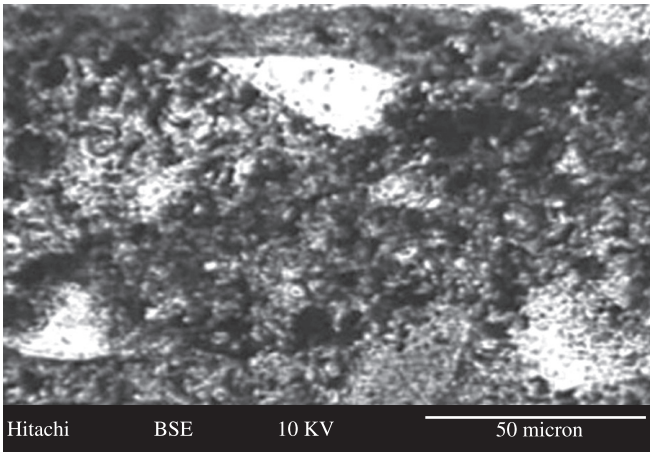

(1)

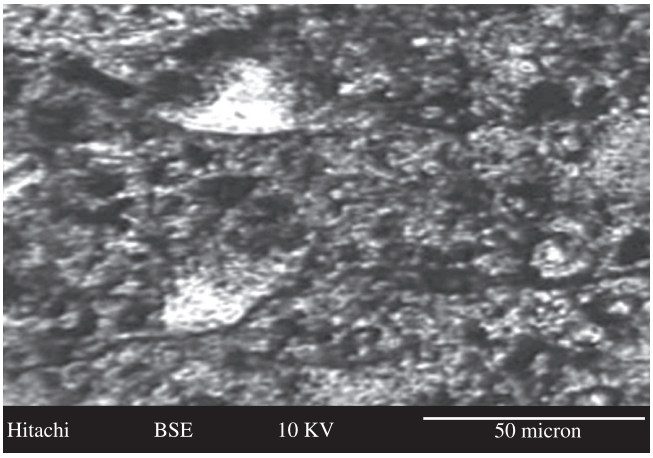

(2)

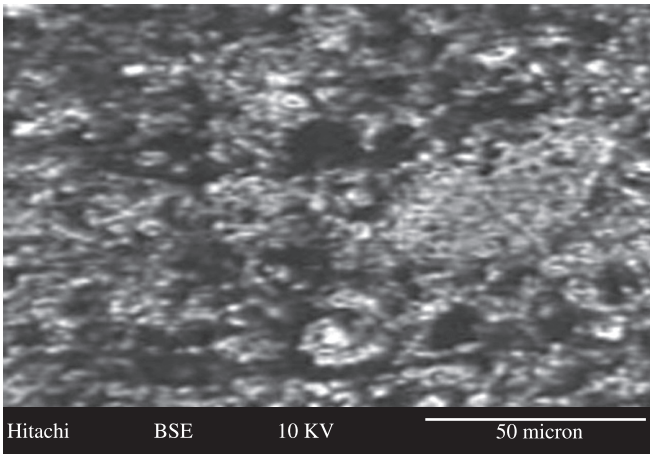

(3)

Figure 9. SEM micrographs of a) N4-SCC1 specimen at 2 days (1), 7 days (2) and 28 days (3) of curing.

T [K] is the absolute temperature;

K [J/K] is the Bultzman's constant;

A is a constant; and

N_T is the number of nucleation sites.

In a constant temperature, by increasing N_T (the smaller nanoparticles) the rate of C-S-H gel formation is increased causes shorter early age.

In general, the free energy of heterogeneous nucleation from gel on the surface of a foreign particle (ΔG_{het} which here is ZrO_2 in the form of aggregate or nanoparticle) could be obtained from Equation 2[61,62];

$$\Delta G_{het} = -V_S.\Delta G_V + A_{sg}.\gamma_{sg} + A_{sp}.\gamma_{sp} - A_{sp}.\gamma_{pg} \quad (2)$$

where:

V_S [cm^3] is the volume of solid nucleus;

ΔG_V [$J.cm^{-3}$] is the volume energy of solid nucleus;

A_{sg} [cm^2] is the interface between solid nucleus and gel;

A_{sp} [cm^2] is the interface between solid nucleus and nanoparticle;

γ_{sg} [$J.cm^{-2}$] is the surface free energy between solid nucleus and gel;

γ_{sp} [$J.cm^{-2}$] is the interface between solid nucleus and nanoparticle; and

γ_{pg} [$J.cm^{-2}$] is the surface free energy between nanoparticle and gel.

The negative signs are due to conversion of gel to solid nucleus. In heterogeneous nucleation, to minimize ΔG^*, the nucleus shape must be a part of hemisphere (Figure 10). The values of V_S, A_{sg} and A_{sp} could be obtained as[61,63]:

$$V_S = \frac{\pi r^3 (2+\cos\theta)(1-\cos\theta)^2}{2\pi r^2 (1-\cos\theta)} \quad (3)$$

$$A_{sg} = 2\pi r^2 (1-\cos\theta) \quad (4)$$

$$A_{sp} = \pi r^2 \sin^2\theta \quad (5)$$

where:

r [cm] is the nucleus radius; and

θ is the wetting angle and is constant during the growth of nucleus (Figure 10).

Figure 10 shows that the equilibrium condition is obtained when[61]:

$$\gamma_{pg} = \gamma_{sp} + \gamma_{pg}\cos\theta \quad \text{or} \quad \cos\theta = \frac{\gamma_{pg} - \gamma_{sp}}{\gamma_{sg}} \quad (6)$$

By substituting of Equations 3 through 6 into Equation 2 one may write[61]:

$$\Delta G_{het} = \left(-\frac{4}{3}\pi r^3 \Delta G_V + 4\pi r^2 \gamma_{sg}\right).S(\theta) \quad (7)$$

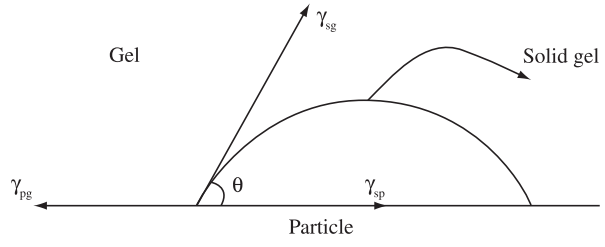

Figure 10. Heterogeneous nucleation of C-S-H gel upon the sands and nanoparticles.

where S(θ) is the shape factor and could be written as[61]:

$$S(\theta)=\frac{(2+\cos\theta)(1-\cos\theta)^3}{4} \quad (8)$$

The critical radius of nucleation (r^*) could be obtained from the first derivative of Equation 7 with respect to r and equaling to zero[61,64]:

$$r^*=\frac{2\gamma_{sg}}{\Delta G_V} \quad (9)$$

By substituting Equation 9 into Equation 7 one may write[61]:

$$\Delta G^*=\frac{16\pi\gamma_{sg}^3}{3\Delta G_V^2}.S(\theta) \quad (10)$$

γ_{sg} and ΔG_V depend on the particle composition and are equal for different particle sizes. Equation 10 shows that by decreasing θ, ΔG^* is also decreased. If both nucleus and nucleation site have the same crystalline structure and have approximately equal cell parameter, then γ_{sp} could be maintained at its minimum amount and according to Equation 6, θ is minimized.

From this point of view, ΔG^* is equal for both nanoparticles and aggregates, but Equation 10 could be written as[61];

$$\Delta G^*=\frac{2}{3}\pi\left(\frac{2\gamma_{sg}}{\Delta G_V}\right)^3.\Delta G_V.\frac{(2+\cos\theta)(1-\cos\theta)^3}{4}= \\ =\frac{\pi\left(r^*\right)^3(2+\cos\theta)(1-\cos\theta)^3}{4}.\frac{1}{2}\Delta G_V=\frac{1}{2}V^*\Delta G_V \quad (11)$$

where:

V^* [cm^3] is the critical volume of nucleus.

The difference between nucleation on aggregates and nanoparticles is in the volume of nucleated material for reaching to r^*. C-S-H gel which is formed around the sand propagates over the time and makes a large amount of C-S-H gel with incoherent interface since its critical volume probably reaches to r^*. On the other hand, nanoparticles do not grow sufficiently and make many dispersed coherent C-S-H gel results in high strength concrete.

4. Conclusions

The results obtained in this study can be summarized as follows:

- The increased the PC content, results in the decreased the split tensile strength. It has been argued that PC retards cement hydration especially at early ages. However no evident differences between split tensile strength of specimens with and without PC.
- As the content of ZrO_2 nanoparticles is increased up to 4 wt. (%), the split tensile strength of SCC specimens is increased. This is due to more formation of hydrated products in presence of ZrO_2 nanoparticles.
- The pore structure of self compacting concrete containing ZrO_2 nanoparticles is improved and the content of all mesopores and macropores is increased.

References

1. Köning G, Holsechemacher K, Dehn F and Weiβe D. Self-compacting concrete-time development of material properties and bond behaviour. In: Ozawa K and Ouchi M, editors. *Proceedings of the 2nd International RILEM Symposium on Self-Compacting Concrete*. Tokyo: COMS Engineering Corporation; 2001. p. 507-516.
2. Hauke B. Self-compacting concrete for precast concrete products in Germany. In: Ozawa K and Ouchi M, editors. *Proceedings of the 2nd International RILEM Symposium on Self-Compacting Concrete*. Tokyo: COMS Engineering Corporation; 2001. p. 633-642.
3. Fava C, Bergol L, Fornasier G, Giangrasso F and Rocco C. Fracture behaviour of self –compacting concrete. In: Wallevik O and Nielsson I, editors. *Proceedings of the 3rd International RILEM Symposium on Self-Compacting Concrete*. Reykjavik: RILEM Publications S.A.R.L.; 2003. p. 628-636.
4. Daoud A, Lorrain M and Laborderie C. Anchorage and cracking behaviour of self-compacting concrete. In: Wallevik O and Nielsson I, editors. *Proceedings of the 3rd International RILEM Symposium on Self-Compacting Concrete*. Reykjavik: RILEM Publications S.A.R.L.; 2003. p. 692-702.
5. Bosiljkov VB. SCC mixes with poorly graded aggregate and high volume of limestone filler. *Cement and Concrete Research*. 2003; 33(9):1279-1286.
6. Makishima O, Tanaka H, Itoh Y, Komada K and Satoh F. Evaluation of mechanical properties and durability of super quality concrete. In: Ozawa K and Ouchi M, editors. *Proceedings of the 2nd International RILEM Symposium on Self-Compacting Concrete*. Tokyo: COMS Engineering Corporation; 2001. p. 475-482.
7. Klug Y and Holschemacher K. Comparison of the hardened properties of self -compacting and normal vibrated concrete. In: Wallevik O and Nielsson I, editors. *Proceedings of the 3rd International RILEM Symposium on Self-Compacting Concrete*. Reykjavik: RILEM Publications S.A.R.L.; 2003. p. 596-605.
8. Chopin D, Francy O, Lebourgeois S and Rougeau P. Creep and shrinkage of heat -cured selfcompacting concrete (SCC). In: Wallevik O and Nielsson I, editors. *Proceedings of the 3rd International RILEM Symposium on Self-Compacting Concrete*. Reykjavik: RILEM Publications S.A.R.L.; 2003. p. 672-683.
9. Felekoðlu B, Türkel S and Baradan B. Effect of water/cement ratio on the fresh and hardened properties of self-compacting concrete. *Building and Environment*. 2007; 42(4):1795-1802.
10. Su N, Hsu K and Chai H. A simple mix design method for self-compacting concrete. *Cement and Concrete Research*. 2001; 31(12):1799-1807.
11. Bjornstrom J, Martinelli A, Matic A, Borjesson L and Panas I. Accelerating effects of colloidal nano-silica for beneficial calcium–silicate–hydrate formation in cement. *Chemical Physics Letters.* 2004; 392(1-3):242-8.
12. Ji T. Preliminary study on the water permeability and microstructure of concrete incorporating nano-SiO2. *Cement and Concrete Research*. 2005; 35(10):1943-7.
13. Jo B-W, Kim C-H, Tae G-h and Park J-B. Characteristics of cement mortar with nano-SiO2 particles. *Construction and Building Materials*. 2007; 21(6):1351-5.
14. Li H, Xiao H-G and Ou J-P. A study on mechanical and pressure-sensitive properties of cement mortar with nanophase materials. *Cement and Concrete Research*. 2004; 34(3):435-8.
15. Li H, Zhang M-H and Ou J-P. Abrasion resistance of concrete containing nanoparticles for pavement. *Wear*. 2006; 260(11-12):1262-6.
16. Qing Y, Zenan Z, Deyu K and Rongshen C. Influence of nano-SiO2 addition on properties of hardened cement paste as compared with silica fume. *Construction and Building Materials*. 2007; 21(3):539-45.
17. Lin KL, Chang WC, Lin DF, Luo HL and Tsai MC. Effects of nano-SiO2 and different ash particle sizes on sludge ash–cement mortar. *Journal of Environmental Management.* 2008; 88(4):708-14.
18. Lin DF, Lin KL, Chang WC, Luo HL and Cai MQ. Improvements of nano-SiO2 on sludge/fly ash mortar. *Waste Manage*. 2008; 28(6):1081-7.
19. Sobolev K, Flores I, Torres-Martinez LM, Valdez PL, Zarazua E and Cuellar EL. Engineering of SiO2 nanoparticles for optimal performance in nano cementbased materials. In: Bittnar Z, Bartos PJM, Nemecek J, Smilauer V and Zeman J, editors. *Nanotechnology in construction*: proceedings of the NICOM3 (3rd international symposium on nanotechnology in construction). Prague, Czech Republic; 2009. p. 139-48.

20. Qing Y, Zenan Z, Li S and Rongshen C. A comparative study on the pozzolanic activity between nano-SiO2 and silica fume. *Journal of Wuhan University of Technology – Materials Science Edition.* 2008; 21(3):153-7.
21. Campillo I, Guerrero A, Dolado JS, Porro A, Ibáñez JA and Goñi S. Improvement of initial mechanical strength by nanoalumina in belite cements. *Materials Letters*. 2007; 61:1889-1892.
22. Li Z, Wang H, He S, Lu Y and Wang M. Investigations on the preparation and mechanical properties of the nano-alumina reinforced cement composite. *Materials Letters*. 2006; 60:356-359.
23. Li H, Xiao H and Ou J. A study on mechanical and pressure-sensitive properties of cement mortar with nanophase materials. *Cement and Concrete Research.* 2004; 34:435-438.
24. Flores-Velez and Dominguez. Characterization and properties of Portland cement composites incorporating zinc-iron oxide nanoparticles. *J Mater Sci*. 2002; 37:983-988.
25. Nazari A, Riahi Sh, Riahi Sh, Shamekhi SF and Khademno A. Mechanical properties of cement mortar with Al_2O_3 nanoparticles. *Journal of American Science.* 2010; 6(4):94-97.
26. Nazari A, Riahi Sh, Riahi Sh, Shamekhi SF and Khademno A. The effects of incorporation Fe_2O_3 nanoparticles on tensile and flexural strength of concrete. *Journal of American Science*. 2010; 6(4):90-93.
27. Nazari A, Riahi Sh, Riahi Sh, Shamekhi SF and Khademno A. Improvement the mechanical properties of the concrete by using TiO_2 nanoparticles. *Journal of American Science*, 2010; 6(4):98-101.
28. Nazari A, Riahi Sh, Riahi Sh, Shamekhi SF and Khademno A. Embedded TiO_2 nanoparticles mechanical properties monitoring in cementitious composites. *Journal of American Science*. 2010; 6(4):86-89.
29. Nazari A, Riahi Sh, Riahi Sh, Shamekhi SF and Khademno A. Benefits of Fe_2O_3 nanoparticles in concrete mixing matrix. *Journal of American Science*, 2010; 6(4):102-106.
30. Nazari A, Riahi Sh, Riahi Sh, Shamekhi SF and Khademno A. Assessment of the effects of the cement paste composite in presence TiO_2 nanoparticles. *Journal of American Science*, 2010; 6(4):43-46.
31. Nazari A, Riahi Sh, Riahi Sh, Shamekhi SF and Khademno A. An investigation on the Strength and workability of cement based concrete performance by using TiO_2 nanoparticles. *Journal of American Science*, 2010; 6(4):29-33.
32. Nazari A, Riahi Sh, Riahi Sh, Shamekhi SF and Khademno A. Influence of Al_2O_3 nanoparticles on the compressive strength and workability of blended concrete. *Journal of American Science*. 2010; 6(5):6-9.
33. ASTM. *ASTM C150. Standard Specification for Portland Cement.* Philadelphia, PA: ASTM; 2001. *Annual book of ASTM standards.*
34. Zivica V. Effects of the very low water/cement ratio. *Const Build Mater* 2009;23(8):2846-2850.
35. ASTM. *ASTM C496. Standard Test Method for Splitting Tensile Strength of Cylindrical Concrete Specimens*. Philadelphia, PA: ASTM; 2001.
36. Abell AB, Willis KL, Lange DA. Mercury intrusion porosimetry and image nalysis of cement-based materials. *Journal of Colloid and Interface Science*. 1999; 211:39-44.
37. Tanaka K and Kurumisawa K. Development of technique for observing pores in hardened cement paste. *Cement and Concrete Research* 2002; 32:1435-41.
38. Roncero J and Gettu R. Influencia de los superplastificantes en la microestructura de la pasta hidratada y en el comportamiento diferido de los morteros de cemento. *Cemento Hormigón.* 2002; 832:12-28.
39. Hans-Ërik G and Pentti P. Properties of SCC-especially early age and long term shrinkage and salt frost resistance. In: Skarendahl Å and Petersson Ö, editors. *Proceedings of the 1st International RILEM Symposium on Self-Compacting Concrete*. Stockholm: RILEM Publications S.A.R.L.; 1999. p. 211-225.
40. Song HW, Byun KJ, Kim SH and Choi DH. Early-age creep and shrinkage in self-compacting concrete incorporating GGBFS. In: Ozawa K and Ouchi M; editors. *Proceedings of the 2nd international RILEM symposium on self-compacting concrete*. Tokyo: COMS Engineering Corporation; 2001. p. 413-422.
41. Hammer TA, Johansen K and Bjøntegaard Ø. Volume changes as driving forces to self-induced cracking of no,rwegian SCC. In: Ozawa K, Ouchi M, editors. *Proceedings of the 2nd International RILEM Symposium on Self-Compacting Concrete*. Tokyo: COMS Engineering Corporation; 2001. p. 423-432.
42. Turcry P and Loukili A. A study of plastic shrinkage of self -compacting concrete. In: Wallevik O and Nielsson I, editors. *Proceedings of the 3rd International RILEM Symposium on Self-Compacting Concrete*. Reykjavik: RILEM Publications S.A.R.L.; 2003. p. 576-585.
43. Heirman G and Vandewalle L. The influence of fillers on the properties of self-compacting concrete in fresh and hardened state. In: Wallevik O, Nielsson I, editors. *Proceedings of the 3rd International RILEM Symposium on Self-Compacting Concrete*. Reykjavik, RILEM Publications S.A.R.L.; 2003. p. 606-618.
44. Ye G, Xiu X, De Schutter G, Poppe AM and Taerwe L. Influence of limestone powder as filler in SCC on hydration and microstructure of cement pastes. *Cement and Concrete Composites*. 2007; 29(2):94-102.
45. Puertas F, Alonso MM and Vázquez T. Effect of polycarboxylate admixtures on portland cement paste setting and rheological behaviour. *Materiales de Construcción*. 2005; 55(277):61-73.
46. Puertas F and Vázquez T. Early hydration cement. Effect of admixtures and superplasticizers. *Materiales de Construcción*. 2001; 51(262):53-61.
47. Puertas F, Santos H, Palacios M and Martínez-Ramírez S. Polycarboxylate superplasticiser admixtures: effect on hydration, microstructure and rheological behaviour. *Advances in Cement Research*. 2005; 17(2):77-89.
48. Wu ZW and Lian HZ. *High performance concrete*. Beijing: Railway Press of China; 1999.
49. Jawed J, Skalny J. and Young JF. *Hydration of portland cement. Structure and performance of cements*. Essex: Applied Science Publishers; 1983. p. 284-285.
50. Mollah MYA, Adams WJ, Schennach R and Cocke DL. A review of cement-superplasticizer interactions and their models. *Advances in Cement Research*. 2000; 12(4):153-161.
51. Yamada K. and Hanehara S. Working mechanism of polycarboxylate superplasticizer considering the chemical structure and cement characteristics. In: *Proceedings of the XI International Conference on the Chemistry of Cement*; 2003; Durban. p. 538-548.
52. Yamada K. and Hanehara S. Interaction mechanism of cement and superplasticizers. The role of polymer adsorption and ionic conditions of aqueous phase. *Concrete Science Engineering*, 2001; 3:135-145.
53. Uchikawa H, Sawaki D and Hanehara S. Influence of kind and added timing organic admixture on the composition, structure and property of fresh cement paste. *Cement and Concrete Research*. 1995; 25(2):353-364.
54. Roncero J, Gettu R and Martın MA. Influencia de los superplastificantes y aditivos reductores de retraccio´n en el comportamiento diferido del hormigo´n estructural. In: *Proceedings of the V Symposium of Asociacio´n Nacional de Fabricantes de Hormigo´n y Mortero*; 2001.
55. Jolicoeur C and Simard MA. Chemical admixture-cement interactions: phenomenology and physico-chemical concepts. *Cement and Concrete Composite*. 1998; 28:87-101.
56. Legrand C. and Wirquin E. Study of the strength of very young concrete as a function of the amount of hydrates formed-influence of superplasticizer. *Materials and Structures*. 1994; 27(166):106-109.
57. Li H, Zhang M and Ou J. Flexural fatigue performance of concrete containing nanoparticles for pavement. *International Journal of Fatigue*. 2007; 29:1292-1301.
58. Ye Q. The study and development of the nano-composite cement structure materials. *New Building Materials.* 2001; (1):4-6.
59. Porter DA and Easteriing KE. *Phase Transformation in Metals and Alloys*. 2nd ed. London: Chapman Hall; 1992.
60. Müller, I. A History of Thermodynamics – the Doctrine of Energy and Entropy. Springer; 2007.
61. Lin YH, Tyan YY, Chang TP and Chang CY. An assessment of optimal mixture for concrete made with recycled concrete aggregates. *Cement and Concrete Research*. 2004; 34(8):1373-1380.
62. Lu P, Young JF. Hot pressed DSP cement paste. *Material Research Society Symposium Proceedings*. 1992; 245.
63. Baierlein, R. *Thermal Physics*. Cambridge University Press; 2003.
64. Reiss, H. *Methods of Thermodynamics*. Dover Publications, 1965.